

Nonlinear coupling in discrete optical waveguide arrays with quadratic nonlinearityFrank Setzpfandt,^{1,*} Wolfgang Sohler,² Roland Schiek,³ and Thomas Pertsch¹¹*Institute of Applied Physics, Abbe Center of Photonics, Friedrich-Schiller-Universität Jena, Max-Wien-Platz 1, 07743 Jena, Germany*²*Angewandte Physik, Universität Paderborn, Warburger Strasse 100, 33095 Paderborn, Germany*³*Ostbayerische Technische Hochschule Regensburg, Prüfening Strasse 58, 93049 Regensburg, Germany*

(Received 17 August 2015; published 26 October 2015)

We demonstrate nonlinear coupling in a discrete optical system. This is achieved in waveguide arrays with quadratic nonlinearity, where the symmetries of the nonlinearly interacting waveguide modes are used to suppress the usually dominating nonlinear effects within individual waveguides. We derive a mathematical model to describe the nonlinear coupling in such waveguide arrays and show experimentally the profound effects of this nonlinear coupling mechanism on second-harmonic generation.

DOI: [10.1103/PhysRevA.92.043832](https://doi.org/10.1103/PhysRevA.92.043832)

PACS number(s): 42.65.Wi, 42.79.Gn, 42.81.Qb

I. INTRODUCTION

Discrete models are routinely used in mathematical physics to predict the behavior of complex physical systems. When describing coherent physical processes in a discrete approximation, the system under investigation is split into several coherent subsystems or oscillators. The state of the system is described by the amplitudes of the eigenmodes of these individual oscillators. Changes to the state of the system happen due to either dissipation or energy exchange between modes. Energy exchange may take place locally between different modes of the individual oscillators or as coupling between modes of different oscillators. In general, both energy exchange channels can linearly or nonlinearly depend on the mode amplitudes. The often assumed linearity of such processes is just an approximation, valid only for small mode amplitudes. In fact, many well-known discrete models include also nonlinear effects, both as locally acting nonlinearities as in the discrete nonlinear Schrödinger equation [1] and as nonlinear coupling. Discrete models with nonlinear coupling include the Fermi-Pasta-Ulam chain [2], used in the first numerical experiment to calculate the motion of a string, and the Ablowitz-Ladik equation [3], which was heavily investigated in mathematical physics for its richness of interesting solutions.

The simple principles of the discrete approximation allow us to describe different physical settings with very similar mathematical models. In recent years, this mathematical similarity has been used to experimentally study otherwise inaccessible systems by investigating more easily accessible model systems. Optical waveguide arrays (WGAs) [4] are a discrete model system with great experimental flexibility due to their geometric variability [5] and the precision in preparing the system as well as the excitation states. Utilizing linear evanescent coupling between neighboring waveguides in WGAs, they have been successfully employed to model electron dynamics in one-dimensional [6,7] and two-dimensional crystals [8,9]. Additionally, WGAs with a local nonlinearity acting in each waveguide are a successful test bed for the predictions made by the discrete nonlinear Schrödinger equation. Most notably, discrete solitons with different dimensionality have been observed experimentally [10–12].

Despite the fact that nonlinear coupling in discrete systems was heavily investigated theoretically [13] and a plethora of interesting phenomena has been described, e.g., solitons [14–16] and breathers [17] as well as their dynamics [18,19] and connections to energy transport in proteins [20], an experimental realization had been missing until now. Several theoretical contributions investigated WGAs in nonlocal nonlinear media [21–23], where nonlinear interactions between several waveguides are possible. These have been realized experimentally in nematic liquid crystals [24,25]. However, since the source of the nonlocality in these structures is the host medium of the WGAs, they cannot be adequately described with a discrete model.

Here we study nonlinear coupling in WGAs induced by the evanescent overlap of waveguide modes with modes of neighboring waveguides. Figure 1(a) shows a scheme of a one-dimensional WGA as considered here. The transversely periodic refractive index profile creating the waveguides is indicated in black. In the discrete approximation, the guided eigenmodes of each waveguide are considered separately and we plot the electric-field profile of waveguide modes of waveguides n and $n + 1$ with the blue lines. The overlap of the evanescent tails of the mode with the neighboring waveguide and its guided modes enables linear coupling between waveguide modes [26]. In nonlinear materials this overlap will also trigger nonlinear interactions between modes of neighboring waveguides. This nonlinear coupling has not yet been investigated, since it naturally is much weaker than local nonlinear interactions within each waveguide due to the stronger fields in the waveguide core.

In this contribution we develop a strategy how nonlinear coupling can be experimentally studied in discrete WGAs with second-order or quadratic nonlinearity. This nonlinearity enables parametric three-wave mixing. In particular, we consider periodically poled WGAs made by titanium indiffusion in lithium niobate [27]. Recently, it has been shown for such WGAs that the use of higher-order waveguide modes enables novel nonlinear effects [28,29]. These higher-order modes are crucial for making the nonlinear coupling accessible experimentally, as they allow us to suppress local nonlinear effects by using their symmetries. We experimentally demonstrate the profound consequences of nonlinear coupling on discrete light propagation by studying second-harmonic generation (SHG), where waveguide modes at the fundamental wave

*Corresponding author: f.setzpfandt@uni-jena.de

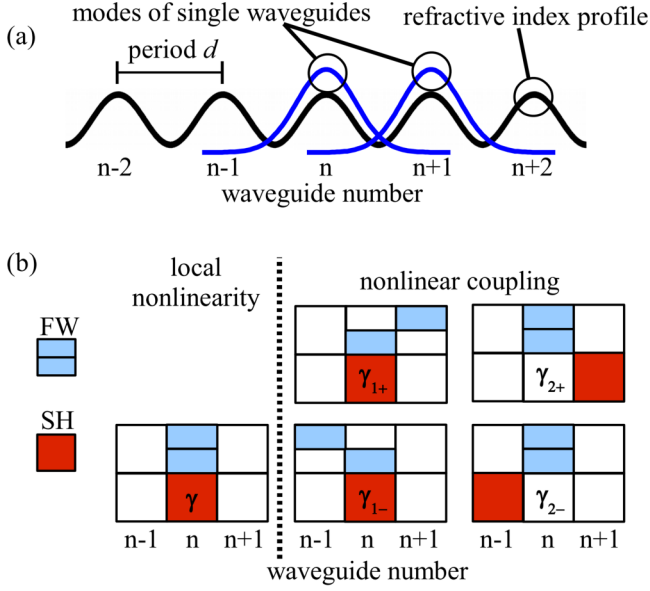


FIG. 1. (Color online) Scheme of the periodic refractive index distribution defining a waveguide array (black) with a mode in one waveguide (blue), showing the evanescent overlap of the electric field of the mode with neighboring waveguides. (b) Interaction chart of different possible nonlinear second-harmonic-generation processes in a waveguide array with nearest-neighbor interaction. Blue rectangles denote one of the fundamental wave modes and red squares the second-harmonic mode. The labels in the individual diagrams denote the coefficient used to describe the respective nonlinear interactions.

(FW) frequency interact with modes at the second-harmonic (SH) frequency obeying $\omega^{\text{SH}} = 2\omega^{\text{FW}}$.

The remainder of this paper is structured in the following way. In Sec. II we analyze theoretically the nonlinear coupling in lithium niobate WGAs. In Secs. III and IV we describe different aspects of our experimental results. Finally, in Sec. V we summarize and discuss various applications of this nonlinear coupling.

II. COUPLED-MODE EQUATIONS

We first develop a mathematical model to describe different SHG interaction mechanisms in WGAs with nonlinear coupling. We restrict our consideration to TM-polarized modes with the main electric-field component along the y direction, parallel to the c axis of the Z -cut lithium niobate WGA used. Considering nonlinear interactions between neighboring waveguides allows for several different spatial positions of the interacting FW and SH modes, which are schematically shown in Fig. 1(b). Up to now, only the local case was investigated, where both FW and the SH components are propagating in the

same waveguide as shown in the left column of Fig. 1(b). The strength of the local nonlinear interaction for TM-polarized modes is quantified by the nonlinear overlap γ [30]:

$$\gamma = \frac{\varepsilon_0}{2\pi P_0} \int_{-\infty}^{\infty} \int_{-\infty}^{\infty} \chi_{333}^{(2)} e_n^{\text{SH}} e_n^{\text{FW}*} e_n^{\text{FW}*} dx dy. \quad (1)$$

Here ε_0 is the dielectric constant, $\chi_{333}^{(2)}$ is the component of the nonlinear tensor that couples TM-polarized electric fields of FW and SH modes, P_0 is the normalization power of the guided modes, and the $e_n^\mu(x, y)$ with $\mu \in \{\text{FW}, \text{SH}\}$ are the electric-field profiles of FW and SH modes in the n th waveguide, respectively.

Spatial combinations of the FW and SH modes resulting from nonlinear coupling are depicted in the two right columns of Fig. 1(b). Here one of the three interacting modes stems from a neighboring waveguide and overlaps with the others just with their evanescent tails. The spatially displaced mode can be either FW or SH and can be shifted to the left or right neighboring waveguide, leading to the four different nonlinear coefficients

$$\gamma_{1\pm} = \frac{\varepsilon_0}{2\pi P_0} \int_{-\infty}^{\infty} \int_{-\infty}^{\infty} \chi_{333}^{(2)} e_n^{\text{SH}} e_n^{\text{FW}*} e_{n\pm 1}^{\text{FW}*} dx dy \quad (2)$$

and

$$\gamma_{2\pm} = \frac{\varepsilon_0}{2\pi P_0} \int_{-\infty}^{\infty} \int_{-\infty}^{\infty} \chi_{333}^{(2)} e_{n\pm 1}^{\text{SH}} e_n^{\text{FW}*} e_n^{\text{FW}*} dx dy, \quad (3)$$

where the local field profiles e_n^μ are the same in each waveguide if a homogeneous WGA is assumed. Nonlinear interactions with all three modes in different waveguides are also possible, but will be neglected here since the interaction strength is orders of magnitude weaker than the nonlinear coupling coefficients derived above.

The considered lithium niobate WGAs are made by titanium indiffusion and consist of waveguides with a transversely symmetric waveguide profile where the refractive index obeys $n(x_0 + x, y) = n(x_0 - x, y)$ with respect to the center of the waveguide x_0 . Consequently, the waveguide modes are either symmetric (even) $e_n^\mu(x_0 + x, y) = e_n^\mu(x_0 - x, y)$ or antisymmetric (odd) $e_n^\mu(x_0 + x, y) = -e_n^\mu(x_0 - x, y)$. Defining a symmetry parameter $S = 1(-1)$ for even (odd) SH modes in this case allows us to reduce the number of nonlinear coupling coefficients

$$\gamma_1 = \gamma_{1+} = S\gamma_{1-}, \quad \gamma_2 = \gamma_{2+} = S\gamma_{2-}. \quad (4)$$

For SHG with equal FW modes as considered here, this simplification is independent of the FW mode symmetry.

Utilizing the nonlinear coefficients described above, we derive the following coupled-mode equations for the propagation of continuous-wave (cw) light in quadratically nonlinear WGAs with nonlinear coupling (see the Appendix A1 for details):

$$\begin{aligned} i \frac{\partial}{\partial z} u_n^{\text{FW}} + i\alpha^{\text{FW}} u_n^{\text{FW}} + c^{\text{FW}} (u_{n-1}^{\text{FW}} + u_{n+1}^{\text{FW}}) &= -\omega_0^{\text{FW}} \gamma u_n^{\text{FW}*} u_n^{\text{SH}} - \omega_0^{\text{FW}} [\gamma_1 (u_{n-1}^{\text{FW}*} u_{n-1}^{\text{SH}} + S u_{n+1}^{\text{FW}*} u_{n+1}^{\text{SH}}) \\ &\quad + \gamma_1 (S u_{n-1}^{\text{FW}*} u_n^{\text{SH}} + u_{n+1}^{\text{FW}*} u_n^{\text{SH}}) + \gamma_2 (S u_n^{\text{FW}*} u_{n-1}^{\text{SH}} + u_n^{\text{FW}*} u_{n+1}^{\text{SH}})], \\ i \frac{\partial}{\partial z} u_n^{\text{SH}} + i\alpha^{\text{SH}} u_n^{\text{FW}} + c^{\text{SH}} (u_{n-1}^{\text{SH}} + u_{n+1}^{\text{SH}}) - \Delta\beta u_n^{\text{SH}} &= -\omega_0^{\text{FW}} \gamma u_n^{\text{FW}*} u_n^{\text{FW}*} - \omega_0^{\text{FW}} [2\gamma_1 u_n^{\text{FW}} (S u_{n-1}^{\text{FW}} + u_{n+1}^{\text{FW}}) + \gamma_2 (u_{n-1}^{\text{FW}*} + S u_{n+1}^{\text{FW}*})] \end{aligned} \quad (5)$$

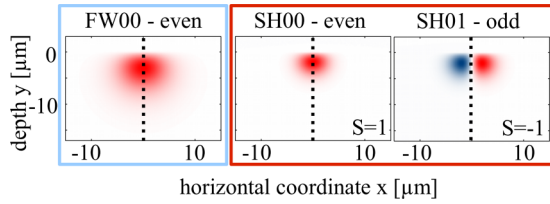


FIG. 2. (Color online) Electric-field profiles of the first-order FW00 (left) and first- and second-order SH00 and SH01 modes for a single waveguide of the waveguide array used in our experiments. The dashed lines denote the symmetry axes at $x = x_0 = 0$.

Here the u_n^μ are the slowly varying amplitudes of FW and SH modes in the n th waveguide, c^μ are the respective linear coupling constants, α^μ are the loss coefficients, and $\Delta\beta$ is the phase mismatch between the interacting modes. The first terms on the right-hand sides of the two equations (5) describe local SHG in WGAs [28]. The terms in the square brackets appear due to the nonlinear coupling.

To estimate the strength of the various nonlinear interactions we numerically obtain mode profiles of FW and SH modes of the WGA used in the experiments (see the Appendix, A3 for details). Results for the electric field of TM-polarized modes at wavelengths of 1500 nm (FW) and 750 nm (SH) are shown in Fig. 2. We find that the first-order FW and SH modes FW00 and SH00, respectively, are even. The next-higher-order mode SH01 is odd. In general, a propagating FW mode can interact simultaneously with several SH modes [31], where the strength of the interaction is controlled by the wavelength-dependent phase mismatches. Optimal SHG efficiency with a certain SH mode can be achieved for vanishing phase mismatch $\Delta\beta$, which we experimentally realize by selecting a suitable FW wavelength [32]. The phase-matching wavelengths of SHG between the FW00 mode and SH00 and SH01 modes are around 1520 and 1500 nm respectively. The period of our WGA sample is $d = 12.5 \mu\text{m}$, leading to linear coupling constants of $c^{\text{FW}} = 360 \text{ m}^{-1}$ for the FW and $c^{\text{SH}} = 154 \text{ m}^{-1}$ for the SH01 mode. The SH00 mode is not coupled due to its highly localized mode profile. Based on the geometric parameters of the WGA and the simulated mode profiles, we calculate the nonlinear coefficients defined above for the respective phase-matching wavelengths, which are summarized in Table I. For SHG with the even SH00 mode, the local nonlinear coefficient is two orders of magnitude larger than the nonlinear coupling coefficients. Hence, the local contributions dominate the nonlinear interactions, resembling the case that was intensively studied in the past. However, for SHG with the SH01 mode the local nonlinear coefficient

TABLE I. Local nonlinear coefficients and nonlinear coupling coefficients for the interaction of the FW00 with the first two SH modes SH00 and SH01. The coefficients are calculated for the phase-matching wavelengths given in the second column.

Mode	Wavelength (nm)	γ (as/m)	γ_1 (as/m)	γ_2 (as/m)
SH00	1520	22980	328	25
SH01	1500	0	320	-78

vanishes since the overlap (1) is always zero for odd SH modes. This suppression of the local nonlinearity enables the experimental observation of nearest-neighbor nonlinear coupling.

We note that due to fabrication tolerances in realistic waveguides, we cannot expect an absolutely symmetric refractive index profile. Hence, a small residual local nonlinearity is expected, but will be neglected in our simulations. This is justified also by our experimental system; the used waveguides made by titanium indiffusion are very symmetric, as will be confirmed by our measurements.

In the following we discuss and experimentally demonstrate two key features of the nonlinear coupling for the experimentally accessible case of SHG with the FW00 and SH01 modes depicted in Fig. 2. These features are the dependence of the generated SH on the FW beam symmetry and a nonlinear anisotropy resulting from such a symmetry constraint.

III. SYMMETRY DEPENDENCE OF SECOND-HARMONIC GENERATION

For SHG to the SH01 mode the generated SH fields in the left- and right-hand nearest neighbors of a particular waveguide n have a phase difference of π due the electric-field profile of the SH01 mode. The symmetry parameter is $S = -1$ and the nonlinear coupling terms in Eqs. (5) are all differences between FW amplitudes residing in the nearest neighbors of the considered waveguide. For an FW beam exciting several waveguides, which is locally symmetric around waveguide n_0 with $u_{n_0+1}^{\text{FW}} = u_{n_0-1}^{\text{FW}}$, no SH is generated in n_0 since the contributions from the neighbor waveguides interfere destructively. Furthermore, for FW beams with global symmetry, where $u_{n_0-n}^{\text{FW}} = u_{n_0+n}^{\text{FW}}$ for all n , SH generated at equal distances from the center waveguide n_0 will destructively interfere in n_0 . This leads to a complete absence of SH in the central waveguide n_0 in this case.

We experimentally show the symmetry dependence of the nonlinear coupling by investigating SHG in the SH01 mode with FW00 excitation in only one waveguide. In this case, the FW undergoes discrete diffraction [26]. The resulting FW intensity distribution is symmetric with respect to the excitation site for all propagation distances. In the WGA being tested, the phase-matching wavelength to the SH01 mode in a single waveguide is 1496.7 nm. For excitation of the FW00 mode in waveguide $n_0 = 0$, the measured SH output intensity distribution, integrated over the vertical y direction, is shown in Fig. 3(a) dependent on the FW wavelength. Since different components of the FW angular spectrum are phase matched at different wavelengths within the measurement range [32], a complicated spatio-spectral pattern arises. Owing to the symmetric FW evolution, the measured SH intensity is symmetric with respect to the input waveguide. Contrary to our expectations, we find SH also in the excitation waveguide.

To determine the modal content of the generated SH we investigate the two-dimensional SH intensity distributions. Figure 3(b) shows an image of the SH intensity distribution for an FW wavelength of 1496.7 nm, corresponding to the slice indicated by the solid white line in Fig. 3(a). The mode profiles measured in almost all waveguides resemble the two-peaked intensity distribution of the SH01 mode, which can only be

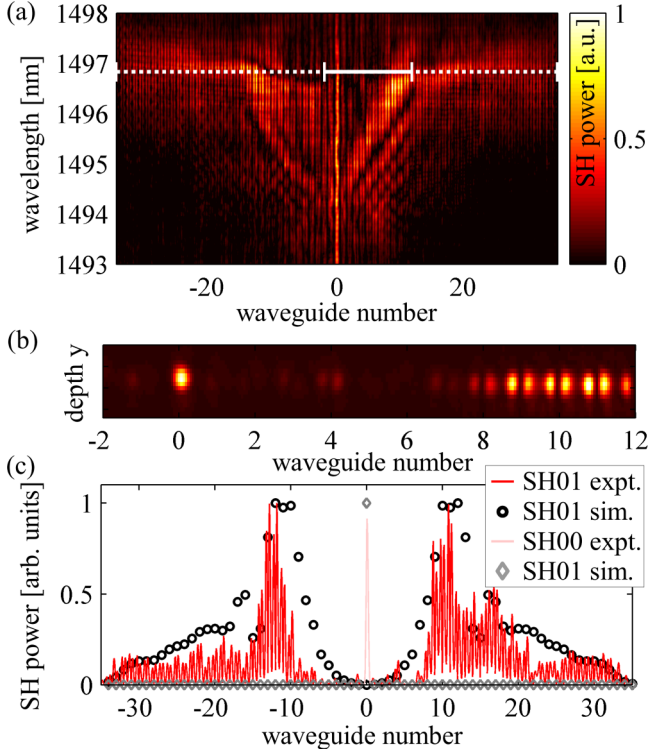


FIG. 3. (Color online) (a) Spatially resolved normalized SH output power of the WGA for single-waveguide FW excitation in waveguide 0 dependent on the FW wavelength. (b) Intensity distribution of SH waveguide modes for FW excitation wavelength of 1496.7 nm. The shown waveguides are indicated by the solid white line in (a). (c) Normalized SH power at the same wavelength as in (b), as indicated by the dotted white line in (a). Depicted are experimental results [black (gray) lines] and simulation of SHG to the SH01 mode (black circles) and SH00 mode (gray diamonds).

generated in the presence of nonlinear coupling. However, the mode in waveguide 0 is an SH00 mode with just a single intensity maximum; no SH01 is present. In Fig. 3(c) we plot the SH power at the phase-matching wavelength, corresponding to the dotted white line in Fig. 3(a), with the red line and compare it with simulations. The power in the central waveguide, which is carried by the SH00 mode, is shown by the light red line. Our simulations take into account SHG to the SH01 mode using Eqs. (5) and to the SH00 mode using the usual coupled-mode equations with local nonlinearity [31]. The simulation results for the SH01 mode (black circles) and for the SH00 mode (gray diamonds) agree very well with the measurement. In particular, the expected suppression of the SH01 mode in the central waveguide, a clear signature of the nonlinear coupling underlying the generation of the SH01 mode, is found in both experiment and simulation. Additionally, the appearance of the SH00 mode in only the central waveguide is also reproduced by the simulations. Although strongly phase mismatched with an expected phase-matching wavelength of around 1520 nm, the SH00 mode is generated due to its large local nonlinear coefficient. It is generated only in the central waveguide, where the exciting FW power propagates only for a short distance before being coupled to the neighboring waveguides due to strong discrete diffraction. Thus, the interaction length

between the FW00 and SH00 modes is on the order of only one coupling length [33], leading to an effectively relaxed phase-matching condition and enhanced generation efficiency.

IV. NONLINEAR ANISOTROPY

The dependence of nonlinear coupling on the FW beam symmetry leads to an anisotropy of the nonlinear interaction strength for SHG from FW discrete plane waves, which we experimentally demonstrate in the following. Discrete plane waves of the form $u_n^\mu(z) = w_0^\mu(z) \exp(i\kappa^\mu n + ik^\mu z)$ are the eigenmodes of the WGA with weak linear coupling. Here w_0^μ are the plane-wave amplitudes, whereas κ^μ and k^μ are the transverse and longitudinal wave numbers, respectively. For $\kappa^{\text{FW}} = m\pi$, $m \in \mathbb{Z}$, FW plane waves are locally (and globally) symmetric with respect to all waveguides and nonlinear coupling into the SH01 mode is completely suppressed. However, for other transverse propagation constants, i.e., other propagation directions of the discrete plane waves, this particular symmetry is lifted and SHG due to nonlinear coupling is expected.

To investigate this anisotropy more rigorously, we derive coupled-mode equations for the amplitudes of the plane waves with nonlinear coupling and $S = -1$. To this end we insert the definitions of the discrete plane waves into the coupled-mode equations (5) and find a new set of coupled-mode equations for the amplitudes of the plane waves. Under the assumption of transverse phase matching $\kappa^{\text{SH}} = 2\kappa^{\text{FW}}$ these are

$$i \frac{\partial}{\partial z} w_0^{\text{FW}} + i\alpha^{\text{FW}} w_0^{\text{FW}} = -\omega_0^{\text{FW}} \gamma_{\text{pw}}^* w_0^{\text{FW}*} w_0^{\text{SH}},$$

$$i \frac{\partial}{\partial z} w_0^{\text{SH}} + i\alpha^{\text{SH}} w_0^{\text{SH}} - \Delta\beta w_0^{\text{SH}} = -\omega_0^{\text{FW}} \gamma_{\text{pw}} w_0^{\text{FW}2}. \quad (6)$$

We find an effective nonlinear coefficient

$$\gamma_{\text{pw}}(\kappa^{\text{FW}}) = 4i\gamma_1 \sin(\kappa^{\text{FW}}) - 2i\gamma_2 \sin(2\kappa^{\text{FW}}), \quad (7)$$

where the local nonlinearity γ is neglected. As expected, the strength of the nonlinear interaction between FW and SH plane waves, which is mediated by the nonlinear coupling, depends on the transverse wave number κ^{FW} . The imaginary part of the effective nonlinear coefficient γ_{pw} is plotted in Fig. 4(a), where we used the parameters of Table I for the FW00 and SH01 modes. Indeed, the nonlinearity is 0 for transverse wave numbers of 0 and $\pm\pi$. The largest nonlinear interaction is expected for $\kappa^{\text{FW}} = \pm \arccos[(\gamma_1 - \sqrt{\gamma_1^2 + 2\gamma_2^2})/2\gamma_2]$, which for the parameters used in Fig. 4 is about $\kappa^{\text{FW}} = \pm 0.46\pi$. The nonlinear interaction strength γ_{pw} is purely imaginary and hence SHG induces a phase shift of $\pi/2$ to the SH wave with respect to the FW.

We measured SHG to the SH01 mode with a broad Gaussian FW00 excitation approximating a plane wave in the same WGA as used before. To control the transverse wave number of the FW beam, the excitation is tilted. The integrated SH power generated in all waveguides dependent on FW transverse wave number κ^{FW} and FW wavelength is shown in Fig. 4(b). As previously shown for SHG with local nonlinearity, the phase-matching wavelength depends strongly on the FW transverse wave number [32]. The expected phase-matching wavelength of FW00 and SH01 plane waves is indicated by the white

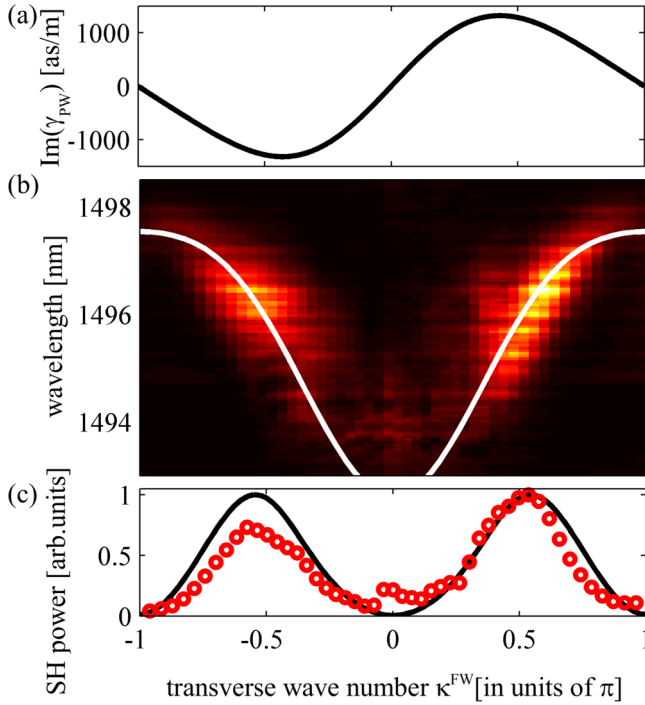


FIG. 4. (Color online) (a) Imaginary part of the effective nonlinear coefficient for SHG of discrete plane waves. The interacting modes are FW00 and SH01 with the nonlinear coupling coefficients of Table I. (b) Second-harmonic power dependent on FW transverse wave number and FW wavelength for SHG of plane waves. The white line indicates simulated phase-matching wavelengths to SH01 plane waves with $\kappa^{\text{SH}} = 2\kappa^{\text{FW}}$. (c) Normalized SH power integrated over the wavelength range shown in (b). Depicted are experimental (red circles) and simulation results (black line).

line and corresponds well to the measured power maxima. Strong SH generation is found for wave numbers around the expected maximum of the nonlinear coefficient. We compare our measurement results, integrated over the investigated wavelength range, with simulations of the coupled-mode equations (5). The results agree very well and are plotted in Fig. 4(c) with the red circles and a black line, respectively. A measured residual SH at $\kappa^{\text{FW}} = 0$ can be explained by differences between the waveguides that break the symmetry of the exciting FW wave, thus enabling SHG. The maximum of the SH power in measurement and simulation appears for transverse wave numbers of $\kappa^{\text{FW}} \approx 0.55\pi$, slightly larger than expected from the analytic expression of the effective nonlinearity plotted in Fig. 4(a). This is due to experimental shortcomings. In contrast to a spatially infinitely extended plane wave, the experimental FW beam has a Gaussian shape with a finite full width at half maximum of eight waveguides. Hence, diffraction and spatial walkoff influence the efficiency of SHG and lead to a shift of the efficiency maximum.

V. CONCLUSION

We described nonlinear coupling between nearest-neighbor waveguides in discrete WGAs. We proposed to employ mode symmetries to control local nonlinear effects in each

waveguide, thus enabling experimental access to the nonlinear coupling. Owing to the properties of our experimental system, WGAs in lithium niobate, our description considered the case of symmetric waveguides, where the modes are either symmetric or antisymmetric. For waveguides with arbitrary refractive index profiles a more general description using all four nonlinear coupling coefficients is necessary. Designing such waveguides would allow us to control the strengths of the nonlinear coupling coefficients individually. Furthermore, in this case local nonlinearities and nonlinear couplings could be designed to have comparable strengths, allowing for the study of their interplay.

In experiments measuring SHG from FW00 to SH01 modes we were able to prove the action of the nonlinear coupling. This embodies an experimental realization of a discrete system with nonlinear coupling, similar to the often-used Ablowitz-Ladik equation. By using cascading [34], nonlinear coupling could also be studied in WGAs with an effective third-order nonlinearity. We expect for such settings to support spatial stationary states, the properties of which could be the topic of further studies.

Specifically, we could experimentally show the predicted dependence of SHG on the beam symmetry and the resulting nonlinear anisotropy. Such symmetry dependence is not known for SHG in WGAs with nonlinearities only within the waveguides. The dependence of the generated SH on the FW beam symmetry could find applications in nonlinear signal analysis. It prohibits the generation of a SH from spatially homogeneous FW signals, allowing for SHG only at inhomogeneities in intensity or phase of the exciting beam. As such, the nonlinear coupling could be used for all-optical edge detection in propagating beams in a similar way as vortex beams are used in microscopy for the discrimination of inhomogeneities in imaged samples [35].

We believe that this nonlinear effect will be of interest in many discrete systems where mode symmetries could be used in nonlinear interactions. Examples may include the generation of discrete solitons, photon pair generation with spontaneous parametric down-conversion in waveguide arrays [36], or even nonlinear effects in Bose-Einstein condensates [37]. Furthermore, WGAs with such nonlinear coupling may be used to simulate other yet inaccessible systems with discrete nonlinear coupling, e.g., arrays of QED cavities [38] or lattice gauge theories [39].

ACKNOWLEDGMENTS

We acknowledge Andrey A. Sukhorukov and Alexander S. Solntsev for helpful discussion. This work was supported by funding from the Carl-Zeiss-Foundation and the German Research Foundation (Program No. DFG SPP 1391 Ultrafast Nanoptics).

APPENDIX

1. Derivation of coupled-mode equations and coefficients

To derive our discrete propagation equations (5) we closely followed the standard approach described in Ref. [30] using the reciprocity theorem. Here we explain only the parts of the derivation concerning the nonlinear coupling. We start from

the master equation describing the dynamics of the amplitude of a waveguide mode \tilde{u} under the action of a slowly varying small perturbation $\Delta\bar{\mathbf{P}}$,

$$i \frac{\partial}{\partial z} \tilde{u}^\mu(z) = -\frac{\omega}{4P_0} \int_{-\infty}^{\infty} \int_{-\infty}^{\infty} dx dy \mathbf{e}^{\mu*}(x,y) \Delta\bar{\mathbf{P}}(\mathbf{r}) e^{(-i\beta^\mu z)}, \quad (\text{A1})$$

where $e^\mu(x,y)$ describes the field profile of the mode μ and β^μ is its propagation constant along the propagation direction z . Assuming SHG where the frequencies of the interacting fields obey $\omega^{\text{SH}} = 2\omega^{\text{FW}}$ and TM polarization for all fields, we can write the nonlinear polarization induced in the n th waveguide by nonlinear interaction with its nearest neighbors as

$$P_n^{(2)}(z) = \varepsilon_0 \chi_{333}^{(2)}(z) \times \sum_{\substack{\mu, \mu' = \text{FW, SH} \\ n', n'' = n-1, n, n+1}} \left[\left(\frac{1}{2} u_{n'}^\mu e_{n'}^\mu e^{(i\beta^\mu z - i\omega^\mu t)} + \text{c.c.} \right) \times \left(\frac{1}{2} u_{n''}^{\mu'} e_{n''}^{\mu'} e^{(i\beta^{\mu'} z - i\omega^{\mu'} t)} + \text{c.c.} \right) \right]. \quad (\text{A2})$$

The z dependence of the susceptibility is due to the quasi-phase-matching (QPM) grating of our samples, created by periodic sign flipping of the nonlinear coefficient with period Λ_{QPM} . We approximate the QPM grating by a cosine function, the first order of its Fourier series. Insertion of Eq. (A2) in Eq. (A1) leads us to the (nonlinear part of the) coupled-mode equations (5), where we used the definitions of the nonlinear coefficients (1)–(3), the phase mismatch $\Delta\beta = 2\beta^{\text{FW}} - \beta^{\text{SH}} + 2\pi/\Lambda_{\text{QPM}}$, and the normalization of the mode amplitude $u_n = \tilde{u}_n \exp(i\Delta\beta z)$.

2. Sample technology

The WGA used in the experiments was manufactured by titanium indiffusion in congruent lithium niobate [27]. In the indiffusion process, 7- μm -wide stripes of titanium with a thickness of 100 nm were indiffused for 8.5 h with a temperature of 1333 K. The waveguides created in this process have very low losses of $\alpha^{\text{FW}} = 0.047 \text{ cm}^{-1}$ and $\alpha^{\text{SH}} = 0.092 \text{ cm}^{-1}$. To enable phase matching in the experimentally accessible wavelength range, a quasi-phase-matching grating with an average period $\Lambda = 16.751 \mu\text{m}$ was created by electric-field poling of the whole sample after the indiffusion process. The average period of the quasi-phase-matching grating was synthesized by using a mixture of two different domain sizes. The utilized WGA had a period of $d = 12.5 \mu\text{m}$ and a length of 51 mm.

3. Mode properties and coefficients

To obtain the properties of the modes and the linear and nonlinear coupling constants used in Eq. (5) we numerically calculated the mode profiles of the waveguides used. The refractive index profile of the waveguides was described by an analytical model for the diffusion of titanium in the lithium niobate host material [40,41]. Necessary input values are the diffusion process parameters given in the preceding section and the diffusion constants $D_x = 4.5 \mu\text{m}^2$ and $D_y = 5.78 \mu\text{m}^2$. Waveguide modes of isolated waveguides with the thus-obtained refractive index profile are calculated by the finite-element method. The nonlinear and linear coupling coefficients were calculated by numerical integration of the calculated modes and refractive index profiles, respectively. To obtain such a coefficient with modes in neighboring waveguides, one of the modes in the calculation was numerically shifted by one WGA period. The calculated nonlinear coefficients are given in Table I; the linear coupling constants are $c^{\text{FW}} = 390 \text{ m}^{-1}$ and $c^{\text{SH}} = 154 \text{ m}^{-1}$. To double-check the simulations we experimentally deduced the FW00 coupling constant from diffraction patterns for single-waveguide excitation, finding a value of $c_{\text{meas}}^{\text{FW}} = 360 \text{ m}^{-1}$, which was used in the simulations together with the other simulated values. The same deviation from the simulations as for the linear FW coupling constant is expected also for the other coefficients used, which does not influence our conclusions.

4. Experimental methods

To generate SHG in WGAs, cw light from a wavelength-tunable diode laser (TUNICS Reference) was coupled into the waveguide array with a 10 \times microscope objective. To excite discrete plane waves, the excitation beam was shaped by a cylindrical lens with a focal length of 300 mm to obtain an elliptical input beam with a horizontal (vertical) full width half maximum diameter of 103(5) μm , exciting eight waveguides simultaneously. The transverse wave number of the FW input was changed by laterally shifting the input beam in front of the coupling objective, thus inducing a tilt in the excitation beam [32]. The FW coupling was controlled by an indium gallium arsenide CCD (XENICS Xeva-1.7-640). Measurements of the SH were performed using a silicon CCD (HAMAMATSU Orca) that could spatially resolve the individual SH modes. Second-harmonic powers were determined by integrating over the measured image. Tuning of the laser wavelength and collection of images were automated to allow for high-resolution wavelength scans.

-
- [1] P. G. Kevrekidis, K. Ø. Rasmussen, and A. R. Bishop, The discrete nonlinear Schrödinger equation: A survey of recent results, *Int. J. Mod. Phys. B* **15**, 2833 (2001).
- [2] E. Fermi, J. Pasta, and S. Ulam, Studies of nonlinear problems, Los Alamos Report LA-1940, 978 (1955).
- [3] M. J. Ablowitz and J. F. Ladik, Nonlinear differential-difference equations, *J. Math. Phys.* **16**, 598 (1975).

- [4] D. N. Christodoulides, F. Lederer, and Y. Silberberg, Discretizing light behavior in linear and nonlinear waveguide lattices, *Nature (London)* **424**, 817 (2003).
- [5] I. L. Garanovich, A. Szameit, A. A. Sukhorukov, T. Pertsch, W. Krolikowski, S. Nolte, D. Neshev, A. Tünnermann, and Y. S. Kivshar, Diffraction control in periodically curved two-dimensional waveguide arrays, *Opt. Express* **15**, 9737 (2007).

- [6] T. Pertsch, P. Dannberg, W. Elflein, A. Bräuer, and F. Lederer, Optical Bloch Oscillations in Temperature Tuned Waveguide Arrays, *Phys. Rev. Lett.* **83**, 4752 (1999).
- [7] H. Trompeter, T. Pertsch, F. Lederer, D. Michaelis, U. Streppel, A. Bräuer, and U. Peschel, Visual Observation of Zener Tunneling, *Phys. Rev. Lett.* **96**, 023901 (2006).
- [8] H. Trompeter, W. Krolikowski, D. N. Neshev, A. S. Desyatnikov, A. A. Sukhorukov, Y. S. Kivshar, T. Pertsch, U. Peschel, and F. Lederer, Bloch Oscillations and Zener Tunneling in Two-Dimensional Photonic Lattices, *Phys. Rev. Lett.* **96**, 053903 (2006).
- [9] M. C. Rechtsman, J. M. Zeuner, A. Tünnermann, S. Nolte, M. Segev, and A. Szameit, Strain-induced pseudomagnetic field and photonic Landau levels in dielectric structures, *Nat. Photon.* **7**, 153 (2013).
- [10] H. S. Eisenberg, Y. Silberberg, R. Morandotti, A. R. Boyd, and J. S. Aitchison, Discrete Spatial Optical Solitons in Waveguide Arrays, *Phys. Rev. Lett.* **81**, 3383 (1998).
- [11] J. W. Fleischer, M. Segev, N. K. Efremidis, and D. N. Christodoulides, Observation of two-dimensional discrete solitons in optically induced nonlinear photonic lattices, *Nature (London)* **422**, 147 (2003).
- [12] S. Minardi, F. Eilenberger, Y. V. Kartashov, A. Szameit, U. Röpke, J. Kobelke, K. Schuster, H. Bartelt, S. Nolte, L. Torner, F. Lederer, A. Tünnermann, and T. Pertsch, Three-Dimensional Light Bullets in Arrays of Waveguides, *Phys. Rev. Lett.* **105**, 263901 (2010).
- [13] Y. S. Kivshar and B. A. Malomed, Dynamics of solitons in nearly integrable systems, *Rev. Mod. Phys.* **61**, 763 (1989).
- [14] B. A. Malomed and J. Yang, Solitons in coupled Ablowitz-Ladik chains, *Phys. Lett. A* **302**, 163 (2002).
- [15] F. Abdullaev, A. Abdumalikov, and B. Umarov, Autosoliton in Ablowitz-Ladik chain with linear damping and nonlinear amplification, *Phys. Lett. A* **305**, 371 (2002).
- [16] M. Öster and M. Johansson, Phase twisted modes and current reversals in a lattice model of waveguide arrays with nonlinear coupling, *Phys. Rev. E* **71**, 025601 (2005).
- [17] S. Aubry, Breathers in nonlinear lattices: Existence, linear stability and quantization, *Physica D* **103**, 201 (1997).
- [18] E. V. Doktorov, N. P. Matsuka, and V. M. Rothos, Dynamics of the Ablowitz-Ladik soliton train, *Phys. Rev. E* **69**, 056607 (2004).
- [19] M. Öster, M. Johansson, and A. Eriksson, Enhanced mobility of strongly localized modes in waveguide arrays by inversion of stability, *Phys. Rev. E* **67**, 056606 (2003).
- [20] K. Kundu, Perturbative study of classical Ablowitz-Ladik type soliton dynamics in relation to energy transport in α -helical proteins, *Phys. Rev. E* **61**, 5839 (2000).
- [21] Y. V. Kartashov, V. A. Vysloukh, and L. Torner, Tunable Soliton Self-Bending in Optical Lattices with Nonlocal Nonlinearity, *Phys. Rev. Lett.* **93**, 153903 (2004).
- [22] A. Fratalocchi and G. Assanto, Discrete light localization in one-dimensional nonlinear lattices with arbitrary nonlocality, *Phys. Rev. E* **72**, 066608 (2005).
- [23] N. K. Efremidis, Nonlocal lattice solitons in thermal media, *Phys. Rev. A* **77**, 063824 (2008).
- [24] A. Fratalocchi, G. Assanto, K. A. Brzdakiewicz, and M. A. Karpierz, Discrete propagation and spatial solitons in nematic-liquid crystals, *Opt. Lett.* **29**, 1530 (2004).
- [25] A. Fratalocchi, G. Assanto, K. A. Brzdakiewicz, and M. A. Karpierz, Discrete light propagation and self-trapping in liquid crystals, *Opt. Express* **13**, 1808 (2005).
- [26] A. L. Jones, Coupling of optical fibers and scattering in fibers, *J. Opt. Soc. Am.* **55**, 261 (1965).
- [27] R. Iwanow, R. Schiek, G. Stegeman, T. Pertsch, F. Lederer, Y. Min, and W. Sohler, Arrays of weakly coupled, periodically poled lithium niobate waveguides: Beam propagation and discrete spatial quadratic solitons, *Optoelectron. Rev.* **13**, 113 (2005).
- [28] F. Setzpfandt, A. A. Sukhorukov, D. N. Neshev, R. Schiek, Y. S. Kivshar, and T. Pertsch, Phase Transitions of Nonlinear Waves in Quadratic Waveguide Arrays, *Phys. Rev. Lett.* **105**, 233905 (2010).
- [29] F. Setzpfandt, A. A. Sukhorukov, D. N. Neshev, R. Schiek, A. S. Solntsev, R. Ricken, Y. Min, W. Sohler, Y. S. Kivshar, and T. Pertsch, Spectral pulse transformations and phase transitions in quadratic nonlinear waveguide arrays, *Opt. Express* **19**, 23188 (2011).
- [30] A. Snyder and J. Love, *Optical Waveguide Theory* (Chapman & Hall, London, 1983).
- [31] F. Setzpfandt, D. N. Neshev, R. Schiek, F. Lederer, A. Tünnermann, and T. Pertsch, Competing nonlinearities in quadratic nonlinear waveguide arrays, *Opt. Lett.* **34**, 3589 (2009).
- [32] F. Setzpfandt, M. Falkner, T. Pertsch, W. Sohler, and R. Schiek, Bandstructure measurement in nonlinear optical waveguide arrays, *Appl. Phys. Lett.* **102**, 081104 (2013).
- [33] T. Pertsch, T. Zentgraf, U. Peschel, A. Bräuer, and F. Lederer, Anomalous Refraction and Diffraction in Discrete Optical Systems, *Phys. Rev. Lett.* **88**, 093901 (2002).
- [34] G. I. Stegeman, M. Sheik-Bahae, E. V. Stryland, and G. Assanto, Large nonlinear phase shifts in second-order nonlinear-optical processes, *Opt. Lett.* **18**, 13 (1993).
- [35] S. Fürhapter, A. Jesacher, S. Bernet, and M. Ritsch-Marte, Spiral phase contrast imaging in microscopy, *Opt. Express* **13**, 689 (2005).
- [36] A. S. Solntsev, F. Setzpfandt, A. S. Clark, C. W. Wu, M. J. Collins, C. Xiong, A. Schreiber, F. Katzschmann, F. Eilenberger, R. Schiek, W. Sohler, A. Mitchell, C. Silberhorn, B. J. Eggleton, T. Pertsch, A. A. Sukhorukov, D. N. Neshev, and Y. S. Kivshar, Generation of Nonclassical Biphoton States Through Cascaded Quantum Walks on a Nonlinear Chip, *Phys. Rev. X* **4**, 031007 (2014).
- [37] O. Morsch and M. Oberthaler, Dynamics of Bose-Einstein condensates in optical lattices, *Rev. Mod. Phys.* **78**, 179 (2006).
- [38] J. Jin, D. Rossini, R. Fazio, M. Leib, and M. J. Hartmann, Photon Solid Phases in Driven Arrays of Nonlinearly Coupled Cavities, *Phys. Rev. Lett.* **110**, 163605 (2013).
- [39] D. Marcos, P. Rabl, E. Rico, and P. Zoller, Superconducting Circuits for Quantum Simulation of Dynamical Gauge Fields, *Phys. Rev. Lett.* **111**, 110504 (2013).
- [40] G. P. Bava, I. Montrosset, W. Sohler, and H. Suche, Numerical modeling of Ti:LiNbO₃ integrated optical parametric oscillators, *IEEE J. Quantum Electron.* **23**, 42 (1987).
- [41] E. Strake, G. Bava, and I. Montrosset, Guided modes of Ti:LiNbO₃ channel waveguides: a novel quasi-analytical technique in comparison with the scalar finite-element method, *J. Lightwave Technol.* **6**, 1126 (1988).